IOP Publishing
Measurement Science and Technology
Meas. Sci. Technol. **31** (2020) 045204 (10pp)
https://doi.org/10.1088/1361-6501/ab5dd9

Role of UV fluence on the thermal regeneration characteristics of fiber Bragg gratings: experiment and analysis

J Kumar[1], O Prakash[1,2], N Choudhary[1,2], R Mahakud[1], S K Dixit[1,2] and S V Nakhe[1]

[1] Raja Ramanna Centre for Advanced Technology, Indore, India
[2] Homi Bhabha National Institute, Mumbai, India

E-mail: jkmadaan@rrcat.gov.in

Received 6 September 2019, revised 22 November 2019
Accepted for publication 2 December 2019
Published 14 January 2020

Abstract

In this paper, the effect of UV exposure time on the thermal regeneration characteristics of fiber Bragg gratings (FBGs) inscribed using 255 nm laser radiation is presented for the first time. This effect is studied in terms of reflectivity, refractive index (RI) modulation and thermal stability of the gratings. Type-I FBGs of RI modulation varying from 2.03×10^{-4} to 3.38×10^{-4} were inscribed in hydrogenated SMF-28 fiber by controlling UV exposure fluence from 0.9 kJ cm^{-2} to 28.8 kJ cm^{-2}. Thermally regenerated gratings were fabricated from type-I FBGs by applying a step-annealing schedule up to 900 °C. The reflectivity of the regenerated FBGs increases with UV fluence and after reaching a maximum value of 46.05%, it decreases. The different behavior of the thermal regeneration characteristics of FBGs is linked with the stress developed inside the fiber during the writing of FBGs and their relaxation during thermal annealing. The theoretical calculations using the defect center and densification model provided an indirect novel approach to estimate the contribution of stress relaxation in thermal regeneration. The work presented in this paper is significant for optimizing the thermal regeneration of FBGs with the final aim of developing a highly reflective regenerated grating for high temperature sensing applications.

Keywords: fiber Bragg grating, thermal regeneration, fiber optics sensors, stress relaxation, UV fluence, defect center, refractive index modulation

(Some figures may appear in colour only in the online journal)

1. Introduction

A fiber Bragg grating (FBG) is an optical device that reflects light of a specific wavelength, depending on its effective refractive index (RI) and the period of modulation that is present within the fiber core [1, 2]. FBGs are used as temperature sensors by monitoring the Bragg wavelength shift with the change in temperature. The Bragg wavelength shift with temperature occurs due to the thermo-optic and thermal expansion coefficients of the fiber material. FBG-based temperature sensing technology has several inherent advantages that make it attractive for a wide range of sensing applications. FBG temperature sensors provide high spatial resolution, single point and distributed sensing capabilities, high sensitivity, faster response time and the capability to work in harsh environments such as nuclear reactor cores, radioactive waste, smelting furnaces and oil industries [1–3]. The thermal stability of an FBG temperature sensor depends on its reflectivity. Decay of reflectivity due to temperature puts a limit on maximum temperature sensing by FBG. Typically, uniform FBGs (type-I) decay significantly for operating temperatures higher than 500 °C [2–4]. FBG temperature sustainability was raised to 800 °C by utilizing tin-doped photosensitive fused silica fiber or by inscribing type-IIa gratings in boron co-doped germanosilicate [5, 6] and germanium-doped fibers [7]. It has been demonstrated that type-IIa FBGs written in germanium

doped photosensitive fiber by 255 nm radiation sustained temperature more than 800 °C [7]. FBGs written with a UV laser beam can sustain temperature up to 800 °C depending upon the exposure time, doping concentration and type of the grating (type-I or type-IIa) [2–8]. Type-II gratings, written by ultrafast fs pulses, can sustain temperatures of more than 1000 °C [9–13]. However, type-II gratings suffer from high transmission losses and poor spectral characteristics [14]. Thermally regenerated FBGs (TRFBGs) from type-I seed grating written in hydrogenated fiber can also go beyond 1000 °C [15–17]. Thermal regeneration is also observed for FBGs written in non-hydrogenated photosensitive optical fiber using nanosecond laser pulses at 248 nm [18]. The thermal regeneration of FBGs has been explained on the basis of stress relaxation at the fiber core–clad interface [18–20]. The thermal regeneration process of type-I FBGs involves diffusion and stress variation due to densification of the fiber core [21]. Surface topography measurements of a regenerated FBG have shown a depression in the core and inner-cladding regions indicating the relaxation of core–cladding interface stresses [22]. The strength of the thermal regeneration depends upon the stress produced inside the fiber during FBG inscription. The stress relaxation at high temperature annealing scales up with the stress induced during inscription [18, 19]. The thermal stability and the lifetime of the FBG depend upon the normalized integrated coupling coefficient which is controlled by the initial reflectivity of the FBG [5]. Similarly, the thermal stability of a thermally regenerated FBG (TRFBG) at any temperature also depends upon the strength of the TRFBG. The thermal regeneration strength depends upon several parameters such as seed FBG strength, grating length, RI modulation, thermal annealing schedule, GeO_2 doping concentration, hydrogen loading, and UV fluence, etc [18–22]. The effect of FBG strength, GeO_2 doping concentration and the annealing schedule on the reflectivity of regenerated gratings has been studied [19, 20]. The maximum reflectivity of a regenerated grating was observed for a seed grating written in H_2 loaded telecommunication grade fiber [19]. The strength of a regenerated FBG scales up with seed FBG reflectivity and RI modulation [20]. The thermal regeneration of an FBG inscribed in double clad non-hydrogenated fiber using frequency-doubled argon–ion laser is also studied [23]. It is shown that the regeneration factor increased by a factor of 1.73 as the fluence increased from 19 kJ cm^{-2} to 44 kJ cm^{-2} [23]. However, a comprehensive study on the role of UV fluence on thermal regeneration characteristics of FBGs written in hydrogenated fiber, and corresponding analysis, is lacking. In the present paper, we have studied the effect of UV fluence on the thermal regeneration characteristics of FBGs written in hydrogenated fibers. Four sets of five FBGs at different UV fluence were inscribed using 255 nm radiation by controlling the UV exposure time. The studies on the thermal regeneration of these gratings were carried out in a step annealing schedule from 600 °C to 900 °C. It was noticed that initially the strength of the regenerated FBG increases with UV fluence and attains the maximum value and then decreases. The thermal regeneration characteristics of the FBGs written with different UV fluence are further analyzed using the defect center and densification model. The contribution of stress relaxation in thermal regeneration is estimated by these experimental and theoretical calculations. These studies will be useful for the maximization of the lifetime of the gratings for the development of high temperature sensors. The sensors presented in this paper are developed with the aim of temperature monitoring of Joule heated ceramic melter for advanced vitrification system. An advanced vitrification system is required for radioactive waste management where the temperature monitoring range varies from 150 °C to 950 °C. The frequent replacement of temperature sensors in such applications can be minimized by using FBG temperature sensors of high thermal stability, as discussed in the present work.

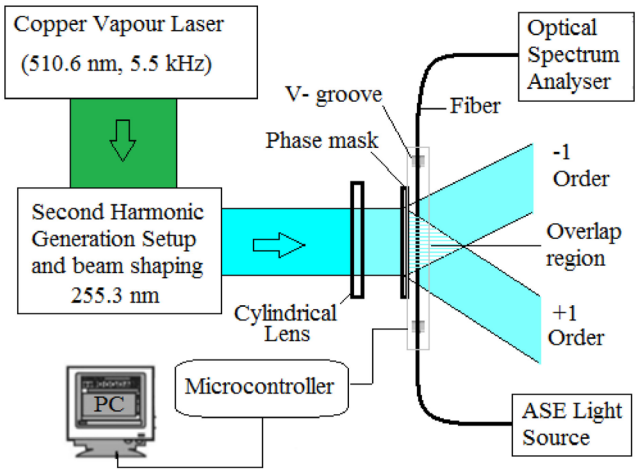

Figure 1. Schematic of FBG inscription using 255.3 nm from CVL.

2. Fabrication of FBGs

A UV beam (wavelength ~255.3 nm, average power ~300 mW, repetition rate ~5.5 kHz) obtained from the second harmonic frequency conversion of copper vapour laser (CVL) radiation (510.6 nm) was used for the inscription of the FBG in hydrogen loaded telecommunication grade SMF-28 silica fiber [7]. Hydrogen loading was completed at a pressure of 100 bar and a temperature of 100 °C for around 144 h (6 d) [24]. The FBGs were written just after the fibers were removed from the hydrogen loading set-up. A schematic of the FBG fabrication using 255.3 nm radiation is shown in figure 1. In the phase mask based inscription technique, the fiber was fixed 0.5 mm behind the phase mask (period = 1060 nm). The UV beam (dimension ~8 mm × 250 μm) was focused on the fiber using a cylindrical lens (focal length ~75 mm). Fringes of spacing of 530 nm were produced on the fiber by the interference between the +1 and −1 diffraction order of phase mask. Growth of the FBG was monitored online using a broadband amplified spontaneous emission (ASE) source (Opto-Link, 1525 nm–1565 nm, with gain flattening filter), 3 dB coupler and optical spectrum analyzer (JDSU-OSA-500). The minimum readout spectral and power resolution of the optical spectrum analyzer (OSA) were 1 pm and 0.01 dB, respectively.

Figure 2 shows the OSA traces recorded for all gratings along with the ASE spectrum (inset). Four sets of five

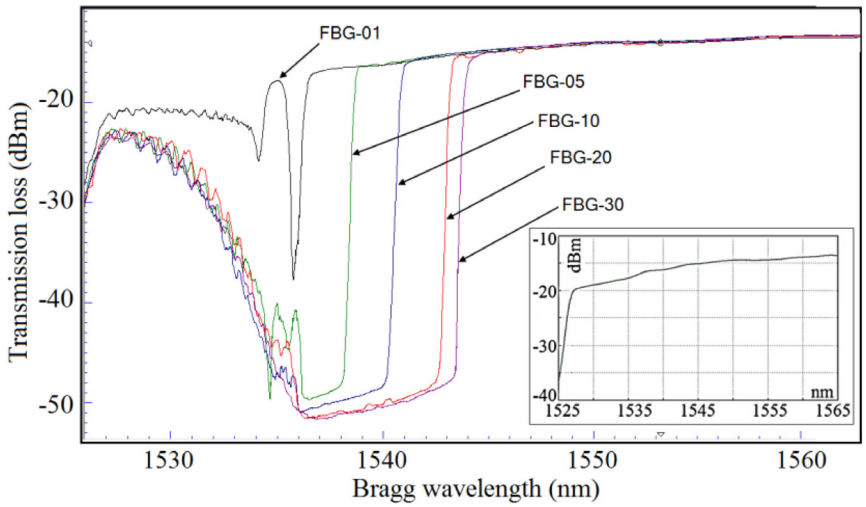

Figure 2. OSA traces for all FBGs inscribed at different UV fluences.

different FBGs were inscribed in hydrogenated SMF-28 fiber by controlling the UV exposure time (t_{exp}). The UV exposure time (t_{exp}) for five FBGs was 1 min, 5 min, 10 min, 20 min and 32 min, respectively. Henceforth, for discussion, we will refer to these gratings as FBG-01, FBG-05, FBG-10, FBG-20 and FBG-30, respectively. The Bragg wavelength of the FBG moves towards the red side with higher transmission dip as the inscription time (cumulative fluence) increases. The reflectivity (R) and Bragg wavelength of 99% (T_d ~ 20 dB) and 1536.075 nm, 99.94% (T_d ~ 32 dB) and 1536.994 nm, 99.96% (T_d ~ 34 dB) and 1538.559, 99.98% (T_d ~ 37 dB) and 1539.671 nm and 99.98% (T_d ~ 37 dB) and 1539.685 nm were recorded for FBG-01, FBG-05, FBG-10, FBG-20 and FBG-30, respectively. The variation of RI modulation (Δn_{ac}) with the cumulative UV fluence (CF) is estimated from the evolution of transmission spectra as [25, 26]:

$$\Delta n_{ac} = \frac{\lambda_B \tan h^{-1}\sqrt{R}}{\eta\, \pi\, L}, \qquad (1)$$

where R is the grating reflectivity, λ_B is the Bragg wavelength, $L = 8$ mm is the grating length and $\eta = 0.9$ is the overlap factor. From figure 3, it is observed that the RI modulation (Δn_{ac}) increases with the UV cumulative fluence. The cumulative UV fluence required for writing FBG-01, FBG-05, FBG-10, FBG-20 and FBG-30 was about 0.9 kJ cm^{-2}, 4.5 kJ cm^{-2}, 9 kJ cm^{-2}, 18 kJ cm^{-2} and 28.8 kJ cm^{-2} respectively. For these fluence values, the RI modulation (Δn_{ac}) of 2.03×10^{-4}, 2.98×10^{-4}, 3.13×10^{-4}, 3.38×10^{-4} and 3.38×10^{-4} was observed for FBG-01, FBG-05, FBG-10, FBG-20 and FBG-30 respectively. The corresponding full width half maxima (FWHM) bandwidth (BW) values for these gratings were 0.47 nm, 2.71 nm, 4.88 nm, 7.22 nm and 7.93 nm respectively. The UV exposure time (t_{exp}), CF, Bragg wavelength (λ_B), reflectivity (R), transmission dip (T_d), RI modulation (Δn_{ac}) and BW values for all these gratings are given in table 1.

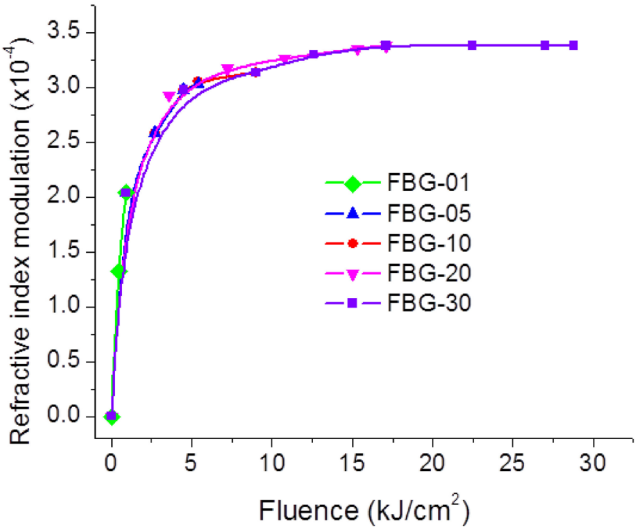

Figure 3. Changes in RI modulation for all FBGs with UV fluence.

3. Thermal regeneration of FBGs

TRFBGs are fabricated by high temperature annealing of all type-I FBGs written in hydrogenated fiber. The gratings were placed inside the heat oven for the observation of thermal regeneration. Regenerated FBG is obtained via a multi-step annealing process of type-I seed gratings up to $T = 900$ °C in four steps with different dwell times [27]. Here the dwell time (t_{dwell}) refers to the resident period of the FBG in the hot zone of the oven maintained at the indicated constant temperature. In the first step $T = 600$ °C was maintained for $t_{dwell} = 240$ min (~4 h), in the second step the temperature was raised to $T = 700$ °C and kept constant for $t_{dwell} = 1020$ min (~17 h), in the third step temperature was further increased to $T = 800$ °C and kept for $t_{dwell} = 240$ min (~4 h), and in the last step the temperature was increased to $T = 900$ °C and kept for $t_{dwell} = 180$ min (~3 h). The transmission dips of all FBGs

Table 1. Parameters of all seed FBGs.

	FBG-01	FBG-05	FBG-10	FBG-20	FBG-30
t_{exp} (minute)	1	5	10	20	32
CF (kJ cm^{-2})	0.9	4.5	9.0	18.0	28.8
λ_B (nm)	1536.075	1536.994	1538.559	1539.671	1539.685
T_d (dB)	20	32	34	37	37
R (%)	99	99.94	99.96	99.98	99.98
BW (nm)	0.47	2.71	4.88	7.22	7.93
$\Delta n_{AC} \times 10^{-4}$	2.03	2.98	3.13	3.38	3.38

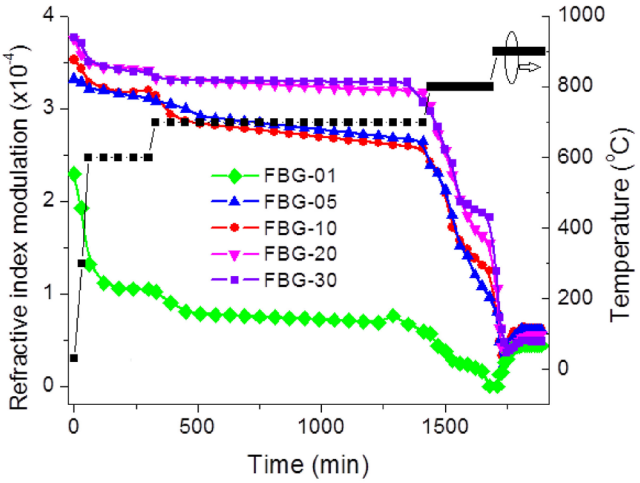

Figure 4. Thermal regeneration of gratings written in hydrogenated fiber.

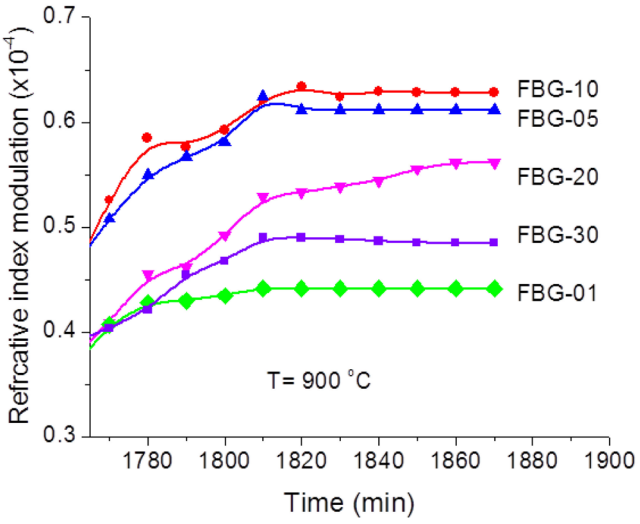

Figure 5. RI modulation during regeneration at 900 °C.

were recorded with different times and temperatures. The RI modulation (Δn_{ac}) was estimated from the transmission dip using equation (1). Figure 4 shows the variation in RI modulation of FBG with different times and temperatures.

The RI modulation of FBG-01 decreased from 2.29×10^{-4} to 1.32×10^{-4} as the temperature increased from room temperature to 600 °C. The RI modulation decreased from 1.32×10^{-4} to 1.05×10^{-4} after 4 h dwelling at 600 °C. As the temperature was raised to 700 °C and kept constant (~17 h) at 700 °C the modulation became 0.67×10^{-4}. This modulation almost decayed as the temperature was kept constant at 800 °C for 3 h. The temperature was further raised to 900 °C. After a 10 min maintenance at 900 °C, the RI modulation again started to increase and reached 0.44×10^{-4} within 3 h at 900 °C. A thermal regeneration of RI modulation ~0.44×10^{-4} was therefore observed in the case of FBG-01. Similarly, thermal regeneration was observed for all FBGs inscribed with different cumulative fluence. RI modulation of the TRFBGs were 0.61×10^{-4}, 0.63×10^{-4}, 0.56×10^{-4} and 0.48×10^{-4} for FBG-05, FBG-10, FBG-20 and FBG-30 respectively. The thermal regeneration temperature for all gratings was 900 °C. It is clear that for all gratings the RI modulation decays initially but at 900 °C, after a certain time, the RI modulation again starts to increase. To clarify the regrowth or regeneration of the RI modulation, an expanded view of figure 4 for the time duration 1760–1870 min is shown in figure 5. Figure 6 shows the OSA traces of all regenerated gratings. The vertical axis is the transmission dip (dBm) and horizontal axis is the wavelength (nm) in figure 6. The Bragg wavelength, reflectivity, RI modulation and FWHM BW at room temperature (~28 °C) are summarized in table 2.

The reflectivity of the TRFBGs were 27.39% (T_d ~ 1.39 dB), 44.41% (T_d ~ 2.55 dB), 46.05% (T_d ~ 2.68 dB), 39.47% (T_d ~ 2.18 dB) and 31.77% (T_d ~ 1.66 dB) for FBG-01, FBG-05, FBG-10, FBG-20 and FBG-30 respectively. The FWHM BW of the regenerated FBGs was 0.31 nm, 0.32 nm, 0.33 nm, 0.33 nm and 0.28 nm for FBG-01, FBG-05, FBG-10, FBG-20 and FBG-30 respectively. The variation in the TRFBG strength (reflectivity and RI modulation) with the cumulative UV fluence required for seed FBG fabrication is shown in figure 7.

These experiments were performed with four identical FBGs fabricated at each fluence to improve the reliability of the results. The results from the multiple experiments are added as error bars in figure 7. It is clear from the figure that the regeneration strength initially increases with UV fluence but after a certain value of the fluence it decreases further. Similar behavior was observed for all FBGs fabricated at the same fluence. Therefore, the writing beam UV fluence was the only parameter that affected the results of each FBG. To understand the role of regenerated grating strength on temperature sustainability of the FBG, the thermal stability of all TRFBGs was recorded at a temperature of 1000 °C for extended times (~10 h). FBG temperature was increased to 1000 °C within 30 min and maintained for 10 h. It is observed

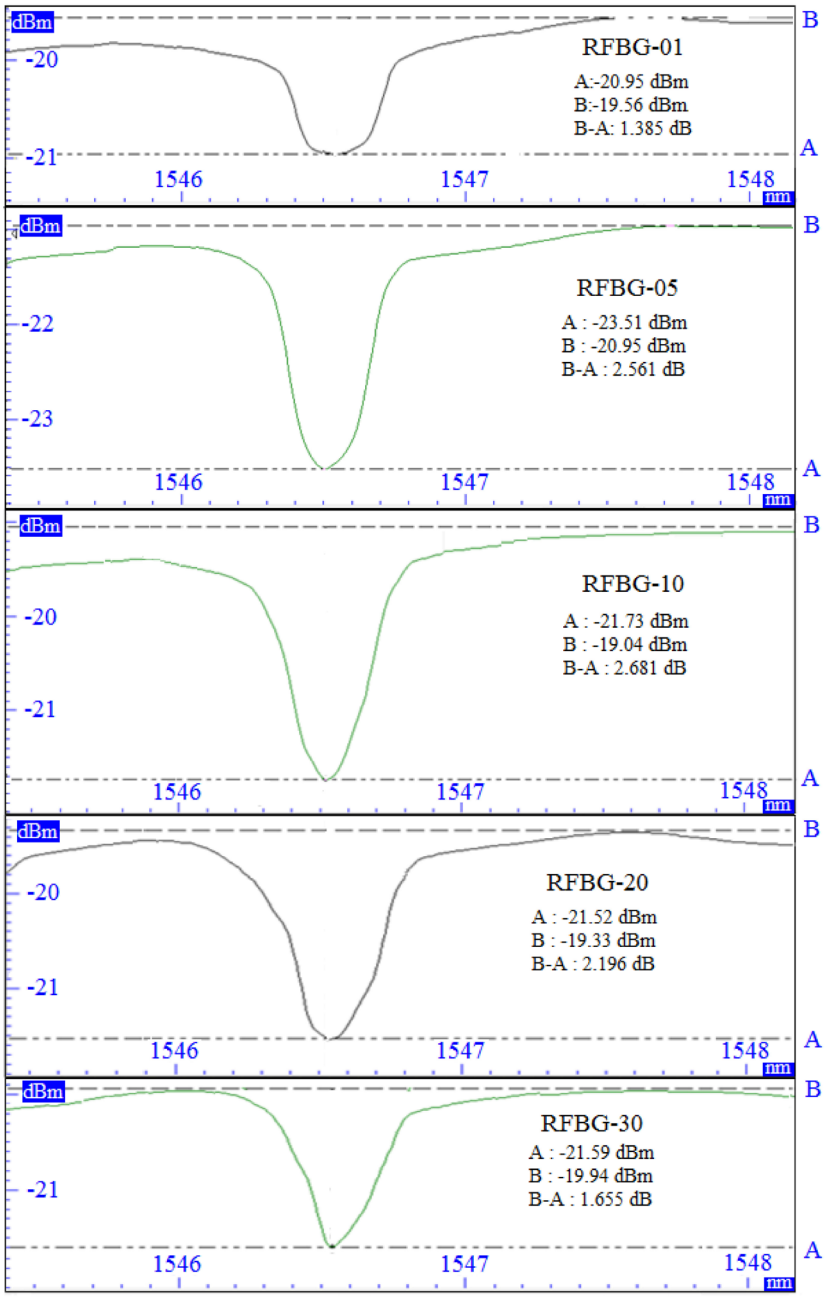

Figure 6. Segments of transmission spectra for all regenerated gratings at 900 °C.

Table 2. Parameters of all regenerated FBGs.

	RFBG-01	RFBG-05	RFBG-10	RFBG-20	RFBG-30
λ_B (nm)	1534.043	1534.012	1534.030	1534.050	1534.004
T_d (dB)	1.39	2.55	2.68	2.18	1.66
R (%)	27.39	44.41	46.05	39.47	31.77
BW (nm)	0.31	0.32	0.33	0.33	0.28
Δn_{AC}	0.44×10^{-4}	0.61×10^{-4}	0.63×10^{-4}	0.56×10^{-4}	0.48×10^{-4}

that the reflectivity initially decreased and then became almost constant at this temperature for all FBGs (as shown in figure 8).

The final constant reflectivity (residual reflectivity) of the gratings at 1000 °C was 15.28% (T_d ~ 0.72 dB), 30.02% (T_d ~ 1.55 dB), 32.39% (T_d ~ 1.70 dB), 27.22% (T_d ~ 1.38 dB) and 22.38% (T_d ~ 1.1 dB) for FBG-01, FBG-05, FBG-10, FBG-20 and FBG-30, respectively. Higher residual reflectivity at higher temperatures in the case of FBG-10 will lead to a higher operational lifetime of the FBG-10 in comparison

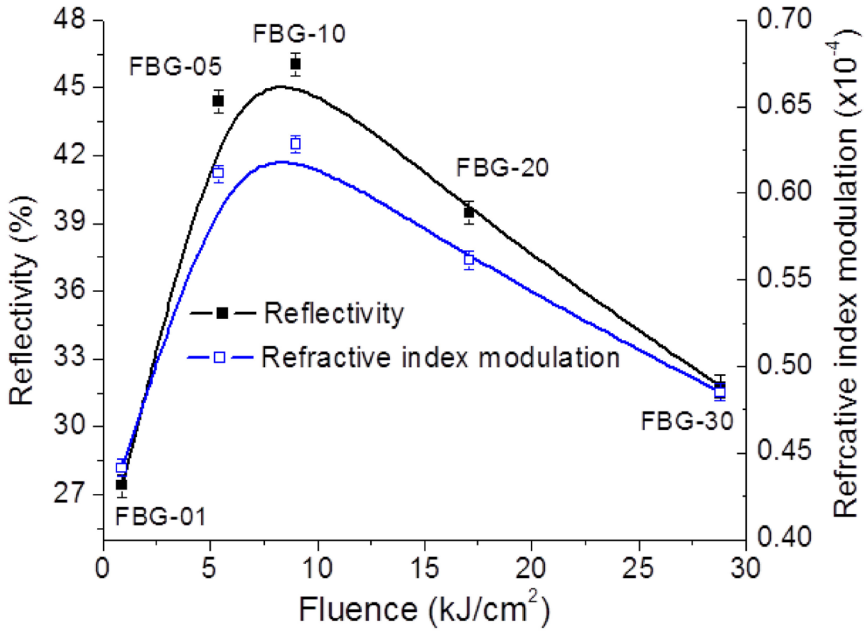

Figure 7. Reflectivity and RI modulation of regenerated FBG as a function of UV fluence required for seed FBG fabrication.

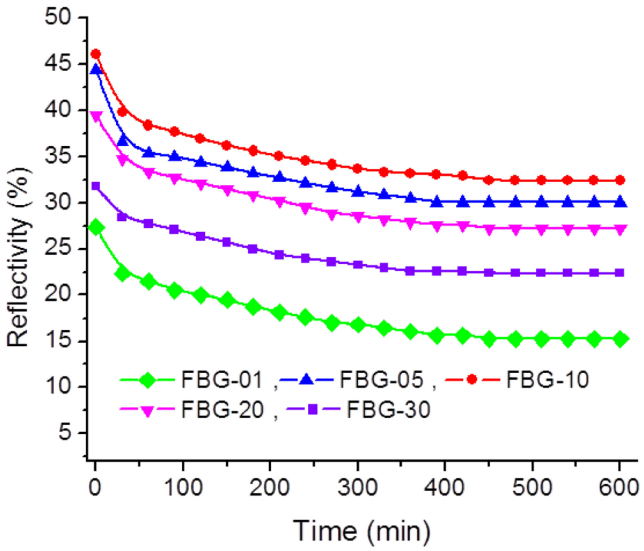

Figure 8. Thermal stability of regenerated gratings at 1000 °C.

with other gratings. The above experiment is therefore useful in deciding the UV fluence required for inscription of an FBG to have a high reflectivity and thermally stable fiber grating.

4. Discussion

The regeneration of an FBG depends upon the seed FBG RI modulation. As the seed FBG modulation increases, the developed stress inside the fiber increases and hence the stress relaxation during high temperature annealing will lead to a regenerated FBG of high modulation [18–22]. In the present experiment, the RFBG strength initially increases with seed FBG modulation, but after attaining an optimum value it decreases. To explain the experimental results of RFBG we have calculated the RI modulation of seed FBG using a defect center model and densification model. From experimental and theoretical results, the contribution of stress induced RI modulation inside the fiber during seed FBG fabrication is estimated. It is observed that RI modulation due to stress relaxation is related with the observed thermal regeneration results. The change in effective RI is a combination of change in effective index due to new defect center formation (δn_{defect}), densification ($\delta n_{\text{densification}}$) and stress ($\delta n_{\text{stress}}$) inside a fiber. During inscription of an FBG, the contribution of δn_{defect} and $\delta n_{\text{densification}}$ is positive and δn_{stress} is negative. The contribution of these parameters can be written as

$$\delta n_{\text{eff}} = \delta n_{\text{defect}} + \delta n_{\text{densification}} + \delta n_{\text{stress}}. \tag{2}$$

The most common model used for the explanation of the formation of FBGs due to UV exposure at 255 nm is the defect center model. According to this model, upon exposure to UV radiation, GeO defect centers in the tetrahedral matrix of the silica host glass break, resulting in the evolution of new defect centers [28–31]. The depletion of GeO defects on UV illumination triggers the formation of trapped states. The excitation of electrons from defect sites (D) induces forbidden transitions to the distribution of trap states (D_1) (called defect induced defects) via an intermediate state (S^1) [32]. The transition of an electron from state D to D_1 depends on the available energy bands with band gap energy corresponding to incidence UV wavelength. The defect center density $N_d(t)$ is given as [33]

$$N_d(t) = N_d(0) \exp(-\beta I t), \tag{3}$$

where $N_d(0)$ is the initial defect center density, I is the UV beam intensity, $\beta = B/c$, B is the transition probability at 255.3 nm and c is velocity of light. The trapped states (D_1) population density, which is equal to the depleted defect centers density, can be given as

$$\Delta N_d(t) = N_d(0)[1 - \exp(-\beta I t)]. \tag{4}$$

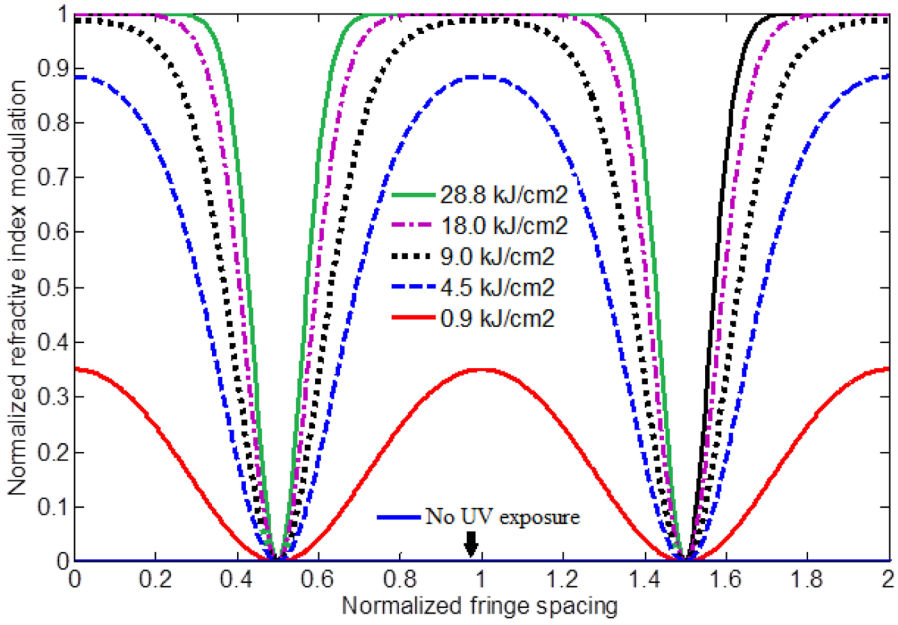

Figure 9. Normalized RI modulation as a function of normalized fringe spacing.

The UV excitation induced RI change in the fiber core increases due to the color-center [34]. Taking the change in RI (δn), linearly proportional to depleted defect center population per unit volume, the induced RI change is described as [33]

$$\delta n(t) = C\,\Delta N_{\mathrm{d}}(t) = C\,N_{\mathrm{d}}\,(0)\,[1 - \exp\,(-\beta\,I\,t)]\,, \quad (5)$$

where C is proportionality constant which depends on the fiber composition. In the case of pulsed laser illumination, the total induced index change is the sum of the incremental index change of successive pulses, given by

$$\delta n = \Delta n_{\max}\,[1 - \exp\,(-\beta N\,I\,t)]\,, \quad (6)$$

where N is the total number of pulses and $\Delta n_{\max} = CN_{\mathrm{d}}\,(0)$ ~ 0.001 is the saturable index change. Now to calculate the UV fringes (sinusoidal) induced RI distribution, the net fringe intensity distribution can be generalized as

$$I\,(z) = I_0\,[1 + \gamma\,\,(x)\,\,\cos\,(2\,\pi\,z/\Lambda)]\,, \quad (7)$$

where Λ is the fringe period, I_0 is the mean fringe intensity, x is the phase mask to the fiber distance and $\gamma(x)$ is the fringe contrast. Using equations (6) and (7), the induced RI distribution across the FBG length is expressed as

$$\delta n\,\,(z) = \Delta n_{\max}\,[1 - \exp\,\{-\beta F\,\,(1 + \gamma\,\,(x)\,\,\cos\,(2\,\pi\,z/\Lambda))\}]\,, \quad (8)$$

where F ($=N\,I_0\,t$) is the accumulated UV fluence. Variation of normalized RI modulation ($\delta n\,\,(z)/\Delta n_{\max}$) with respect to normalized fringe spacing (z/Λ) is calculated from equation (8) and plotted in figure 9. Typical values of the different parameters chosen for the present calculation are the pulse repetition rate = 5.5 kHz, average laser power P_{av} ~ 300 mW, UV beam area = 8 mm × 250 μm, $\beta = 0.24$, $\gamma = 1.0$ and $F = 0.0$ kJ cm^{-2} to 28.8 kJ cm^{-2}.

It is clear from the figure that the RI modulation was initially sinusoidal but as the fluence increases, it starts to deviate from the sinusoidal distribution. At higher fluence, the higher order harmonics of RI modulation may appear and lead to

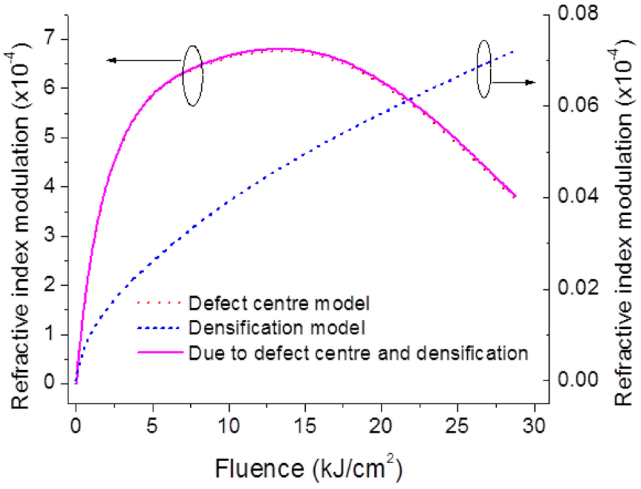

Figure 10. Theoretically calculated results of RI modulation.

fiber gratings with different behaviors. The RI changes $\delta n(z)$, expressed in a Fourier series, is given as

$$\delta n\,\,(z) \approx \langle \delta n \rangle + \,\,\delta n^{(1)}\,\,\cos\,(2\,\pi\,z/\Lambda)\,, \quad (9)$$

where $\langle \delta n \rangle$ and $\delta n^{(1)}$ represents the period averaged and amplitude of the first harmonic component of induced RI, $\delta n(z)$ respectively. By using the exponential series expansion, carrying out necessary integrations and ignoring higher order terms, the Fourier coefficients $\langle \delta n \rangle$ and $\delta n^{(1)}$ of δn(z) are expressed as [33]

$$\langle \delta n \rangle \approx \,\,\Delta n_{\max}\,\,\left[1 - \left\{(1 + 0.25\,\gamma^2\beta^2F^2)\exp(-\beta F)\right\}\right] \quad (10)$$

$$\delta n_{\mathrm{defect}} = \delta n^{(1)} \approx \gamma\beta F\exp\,(-\beta F)\,\,\Delta n_{\max}\,\,\left[1 + 0.125\,\gamma^2\beta^2F^2\right]. \quad (11)$$

It is clear from equations (10) and (11) that the mean index change and RI modulation in different harmonics depend on both fluence and fringe contrast. In figure 9 the first harmonic

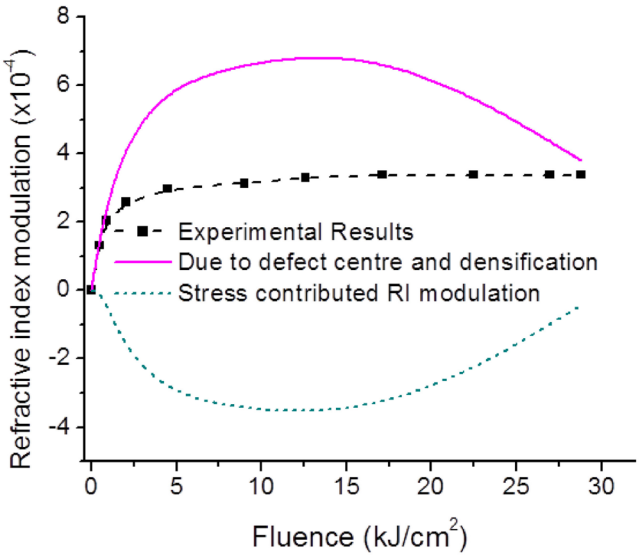

Figure 11. Experimental and theoretical results of RI modulation.

of the RI modulation increases with UV fluence up to 9 kJ cm^{-2} (black dotted line); after this it starts to decrease with increased fluence. Using equation (10) the RI modulation as a function of fluence can be plotted as shown in figure 10. Now, according to the densification model, the glass network bonds are broken by UV radiation leading to compression of glass structure and hence producing RI change [35]. The densification can be described mathematically with a power-law fitting, given as [35, 36]

$$\frac{\Delta\rho}{\rho} = a\left(\frac{N_{\mathrm{M}} I_{\mathrm{d}}^2}{\tau}\right)^{\mathrm{b}}, \tag{12}$$

where N_{M} is the number of pulses (in million), τ is the pulse duration (ns) and I_{d} is the pulse energy density (mJ cm^{-2}) of the UV laser radiation. Here 'a' and 'b' are calculated by the numerical fitting of the experimental data. Typical values for highly photosensitive silica are $a = 45.5$ and $b = 0.57$, at 193 nm UV exposure [36]. So, for the present experiment, the values of the different parameters are UV beam pulse energy density I_{d} =2.18 mJ cm^{-2}, pulse width $\tau = 10$ ns, $a = 45.5$ and $b = 0.57$. For 255 nm radiation, the densification values will be about ten times smaller as those estimated for 193 nm [36, 37]. The change in RI is related to the change in densification by Lorentz–Lorenz equation, such as [38]:

$$\delta n_{\mathrm{densification}} = \left(\frac{\Delta\rho}{\rho}\right)\ (1+\Omega)\ \frac{(n^2-1)\,(n^2+2)}{6n}, \tag{13}$$

where Ω is the ratio of relative polarizability change to the relative density change (~ −0.18) and n is the RI (~1.45) for silica. Figure 10 shows the estimated change in the RI ($\delta n_{\mathrm{densification}}$) as a function of UV fluence.

Figure 11 shows the total RI modulation calculated using the defect center and densification model and experimentally observed RI modulation as a function of UV cumulative fluence. It is clear from the figure that the theoretically calculated results and the experimentally observed value do not match. This therefore indicates that some other factor, such as stress,

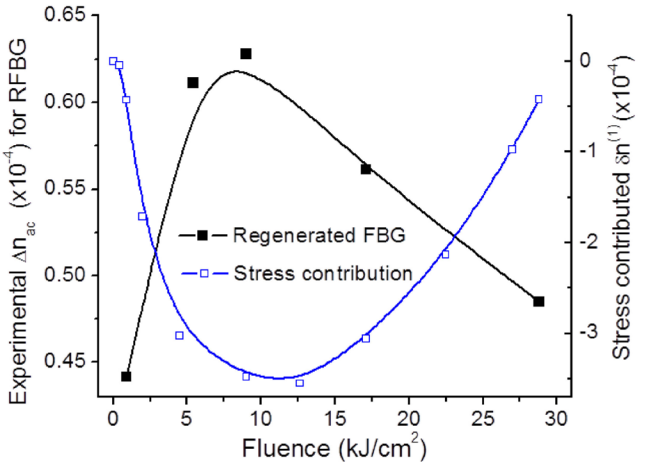

Figure 12. Experimentally observed RI modulation of TRFBG and theoretically calculated stress contribution in seed FBG.

is also responsible for the RI change, in addition to the defect center and densification model. Since the experimental values are lower than the theoretical calculated values, the additional factor should decrease the RI with increase in UV fluence. It is well known that in glass the RI reduces under stress [38]. Therefore, the stress may be the additional factor responsible for the mismatch between the theoretical and experimental values. The deviation in the experimentally observed results from the theoretically calculated results is estimated and shown in figure 11. This deviation is termed as 'stress contributed RI modulation' in the figure.

It is clear from figure 11 that due to stress, the change in RI initially decreases with UV fluence and after attaining a certain value it increases with UV fluence. The maximum deviation is observed in the fluence range of around 9–12 kJ cm^{-2}. Thermal regeneration of the FBG is observed due to stress relaxation inside the fiber. The higher the developed stress in the fiber, the higher the thermal regeneration. In the present case the thermal regeneration of the FBG with UV fluence can also be linked with stress relaxation in the fiber. The variation of experimentally observed RI modulation of TRFBGs and calculated stress contribution in seed FBG with UV fluence is shown in figure 12.

It is clear from the figure that the RI modulation of the TRFBG increases with increase in the magnitude of stress contributed RI modulation. The RI modulation of the TRFBG and the magnitude of the stress contributed RI modulation in seed FBG both are maximum at the UV fluence of around 9 kJ cm^{-2}. As the magnitude of stress contributed RI decreases, the strength of the TRFBG also decreases. Experimentally observed results of the variation of RI modulation of TRFBGs follow the same trends of the variation of magnitude of stress contributed RI modulation in seed FBGs with UV fluence.

5. Conclusion

The thermal regeneration characteristics of the seed FBGs fabricated in hydrogenated telecommunication grade fiber with different UV fluence are studied. The strength of

seed FBGs studied increased monotonically with fluence. However, the strength of regenerated FBGs for different fluence followed a different trend. The reflectivity of regenerated FBGs first increased to the maximum and then decreased with UV fluence. The maximum reflectivity of R ~ 46.05% was observed for seed FBG written at cumulative UV fluence of 9 kJ cm^{-2}. At further higher fluence of 28.8 kJ cm^{-2}, the reflectivity reduced to R ~ 31.77 %. The RI modulation of seed FBGs written at different fluence are analyzed using both defect center and densification model. Contribution of stress to the RI modulation in seed FBG is estimated from the difference between the experimentally observed RI modulation and theoretically calculated values. It was found that the negative of RI modulation attributed due to stress follows the same pattern as the RI modulation of thermally regenerated FBG. The results presented in this paper will be very useful for the development of thermally stable FBG temperature sensors.

ORCID iDs

J Kumar https://orcid.org/0000-0001-9666-8280

References

[1] Canning J 2008 Fibre gratings and devices for sensors and lasers *Laser Photonics Rev.* **2** 275–89
[2] Grattan K T V and Sun T Dr 2000 Fiber optic sensor technology: an overview *Sensors Actuators* A **82** 40–61
[3] Kersey A D, Davis M A, Patrick H J, LeBlanc M, Koo K P, Askins C G, Putnam M A and Friebele E J 1997 Fiber grating sensors *J. Light. Wave Technol.* **15** 1442–63
[4] Canning J, Sommer K and Englund M 2001 Fibre gratings for high temperature sensor applications *Meas. Sci. Technol.* **12** 824–8
[5] Brambilla G and Rutt H 2002 Fiber Bragg gratings with enhanced thermal stability *Appl. Phys. Lett.* **80** 3259–61
[6] Groothoff N and Canning J 2004 Enhanced type IIA gratings for high-temperature operation *Opt. Lett.* **29** 2360–2
[7] Prakash O, Kumar J, Mahakud R, Agrawal S, Dixit S K and Nakhe S V 2014 Enhanced temperature (~800 °C) stability of type IIa fiber Bragg grating written in Ge doped photosensitive fiber *IEEE Photonics Technol. Lett.* **26** 93–5
[8] Fokine M 2002 Thermal stability of chemical composition gratings in fluorine-germanium-doped silica fibers *Opt. Lett.* **27** 1016–8
[9] Grobnic D, Smelser C W, Mihailov S J and Walker R B 2006 Long term thermal stability test at 1000 °C of silica fiber Bragg gratings made with ultrafast laser radiation *Meas. Sci. Technol.* **17** 1009–13
[10] Li Y, Yang M, Wang D N, Lu T, Sun J and Grattan K T V 2009 Fiber Bragg gratings with enhance thermal stability by residual stress relaxation *Opt. Express* **17** 19785–90
[11] Slattery S A, Nikogosyan D N and Brambilla G 2005 Fiber Bragg grating inscription by high intensity femtosecond UV laser light: comparison with other existing method of fabrication *J. Opt. Soc. Am.* B **22** 354–61
[12] Liao C R and Wang D N 2013 Review of femtosecond laser fabricated fiber Bragg gratings for high temperature sensors *Photoelectr. Sensors* **3** 97–101
[13] Mihailov S J and Gover M C 1994 Periodic cladding surface structures induced when recording fiber Bragg grating reflectors with a single pulse from a KrF excimer laser *Appl. Phys. Lett.* **65** 2639–41
[14] Aslund M L, Nemanja N, Groothoff N, Canning J, Marshall G D, Jackson S D, Fuerbach A and Withford M J 2008 Optical loss mechanism in femtosecond laser written point-by-point fiber Bragg gratings *Opt. Express* **16** 14248–54
[15] Bandyopadhyay S, Canning J, Stevenson M and Cook K 2008 Ultrahigh-temperature regenerated gratings in boron-codoped germanosilicate optical fiber using 193 nm *Opt. Lett.* **33** 1917–9
[16] Cook K, Shao L Y and Canning J 2012 Regeneration and helium: regenerating Bragg gratings in helium-loaded germanosilicate optical fibre *Opt. Mater. Express* **2** 1733–42
[17] Canning J, Stevenson M, Bandyopadhyay S and Cook K 2008 Extreme silica optical fiber gratings *Sensors* **8** 6448–52
[18] Lindner E, Chojetzki C, Bruckner S, Becker M, Rothhardt M and Bartelt H 2009 Thermal regeneration of fiber Bragg gratings in photosensitive fibers *Opt. Express* **17** 12523–31
[19] Bandyopadhyay S, Canning J, Biswas P, Stevenson M and Dasgupta K 2012 A study of regenerated gratings produced in germanosilicate fibers by high temperature annealing *Opt. Express* **19** 1198–206
[20] Canning J, Bandypadhyay S, Biswas P, Aslund M, Stevenson M and Cook K 2010 Regenerated fiber Bragg gratings *Frontiers in Guided Wave Optics and Optoelectronics* ed B Pal (Rijeka: InTech) (www.intechopen.com/books/frontiers-in-guided-wave-optics-and-optoelectronics/regenerated-fibre-bragg-gratings)
[21] Celikin M, Barba D, Bastola B, Ruediger A and Rosei F 2016 Development of regenerated fiber Bragg grating sensors with long-term stability *Opt. Express* **24** 21897–909
[22] Lancry M, Cook K, Cao J, Billotte T, Poumellec B and Canning J 2017 Study on stress relaxation in UV regenerated fiber Bragg gratings *IEEE Xplore Conf. on Lasers and Electro-Optics Europe & European Quantum Electronics Conf.* p 17350363 (https://doi.org/10.1109/CLEOE-EQEC.2017.8087290)
[23] Jantzen A, Bannerman R H S, Berry S A, Gates J C, Gow P C, Boyd L J, Smith P G R and Holmes C 2017 Observations from direct UV-written, non-hydrogen-loaded, thermally regenerated Bragg gratings in double-clad photosensitive fiber *Opt. Lett.* **42** 3741–4
[24] Kumar J, Prakash O, Mahakud R, Agrawal S K, Mokhariwale A, Dixit S K and Nakhe S V 2017 Studies on the stability of regenerated fiber Bragg gratings at 1100 °C *IEEE Xplore Workshop on Recent Advances in Photonics* vol **1**6596528 pp 1–4
[25] Kashyap R 1999 *Fiber Bragg Gratings* (New York: Academic)
[26] Nikogosyan D N 2006 Multi-photon high-excitation-energy approach to fibre grating inscription *Meas. Sci. Technol.* **18** R1–29
[27] Kumar J, Prakash O, Mahakud R, Agrawal S K, Dixita S K, Nakhe S V and Canning J 2017 Wavelength independent chemical sensing using etched thermally regenerated FBG *Sens. Actuators* B **244** 54–60
[28] Stone J 1987 Photorefractivity in GeO_2-doped silica fibers *J. Appl. Phys.* **62** 4371–4
[29] Yeun J M 1982 Ultraviolet absorption studies of germanium silicate glasses *Appl. Opt.* **21** 136–40

[30] Poumellec B, Guenot P, Riant I, Sansonetti P, Niay P, Bernage P and Bayon J F 1995 UV induced densification during Bragg grating inscription in Ge:SiO_2 preforms *Opt. Mater.* **4** 441–9
[31] Atkins R M and Mizrahi V 1992 Observations of changes in UV absorption bands of single mode germanosilicate core optical fibres on writing and thermally erasing refractive index gratings *Electron. Lett.* **28** 1743–4
[32] Kristensen M 2001 Ultraviolet-light-induced processes in germanium-doped silica *Phys. Rev.* B **64** 144201
[33] Mahakud R, Prakash O, Nakhe S V and Dixit S K 2012 Analysis on the saturation of refractive index modulation in fiber Bragg gratings (FBGs) written by partially coherent UV beams *Appl. Opt.* **51** 1828–35
[34] Anderson D Z, Mizrahi V, Erdogan T and White A E 1993 Production of in-fibre gratings using a diffractive optical element *Electron. Lett.* **29** 566–8
[35] Borrelli N F, Smith C, Allan D C and Seward T P 1997 Densification of fused silica under 193-nm excitation *J. Opt. Soc. Am.* B **14** 1606–15
[36] Borrelli N F, Smith C M and Allan D C 1999 Excimer-laser-induced densification in binary silica glasses *Opt. Lett.* **24** 1401–3
[37] Schenker R, Schermerhorn P and Oldham W G 1994 Deep-ultraviolet damage to fused silica *J. Vac. Sci. Technol.* B **12** 3275–9
[38] Mueller H 1938 The theory of photoelasticity *J. Am. Ceram. Soc.* **21** 27–33